

UNIVERSITY OF WARWICK

MSc THESIS

---

**Discovery of a Hot Jupiter around a  
G5V star with SuperWASP**

---

*Author:*

Jessica SPAKE

*Supervisor:*

Prof. Don POLLACCO

*A thesis submitted in fulfilment of the requirements  
for the degree of MSc by Research*

*in the*

Astronomy & Astrophysics Group  
Department of Physics

October 2016

# Declaration of Authorship

I, Jessica SPAKE, declare that this thesis titled, 'Discovery of a Hot Jupiter around a G5V star with SuperWASP' and the work presented in it are my own. I confirm that:

- This work was done wholly or mainly while in candidature for a research degree at this University.
- Where any part of this thesis has previously been submitted for a degree or any other qualification at this University or any other institution, this has been clearly stated.
- Where I have consulted the published work of others, this is always clearly attributed.
- Where I have quoted from the work of others, the source is always given. With the exception of such quotations, this thesis is entirely my own work.
- I have acknowledged all main sources of help.
- Where the thesis is based on work done by myself jointly with others, I have made clear exactly what was done by others and what I have contributed myself.

Signed:

---

Date:

---

UNIVERSITY OF WARWICK

## *Abstract*

Faculty Name  
Department of Physics

MSc by Research

### **Discovery of a Hot Jupiter around a G5V star with SuperWASP**

by Jessica SPAKE

We report the discovery of a new transiting planet from the WASP survey. WASP-135b is a hot Jupiter with a radius of  $1.30 \pm 0.09 R_J$ , a mass of  $1.90 \pm 0.08 M_J$  and an orbital period of 1.401 days. Its host is a Sun-like star, with a G5 spectral type and a mass and radius of  $0.98 \pm 0.06 M_\odot$  and  $0.96 \pm 0.05 R_\odot$  respectively. The proximity of the planet to its host means that WASP-135b receives high levels of insolation, which may be the cause of its inflated radius. Additionally, we find weak evidence of a transfer of angular momentum from the planet to its star.

# Acknowledgements

I would like to thank the following collaborators without whom this work would have been impossible. This list includes the names of everyone involved in SuperWASP, and the names of people who have directly contributed to this work (the specific contributions are highlighted in the main text of this thesis). I would especially like to thank my supervisor Don Pollacco, to whom I owe a great deal.

D. J. A. Brown<sup>1</sup>, A. P. Doyle<sup>1</sup>, G. Hébrard<sup>2,3</sup>, J. McCormac<sup>1</sup>, D. J. Armstrong<sup>1,4</sup>, D. Pollacco<sup>1</sup>, Y. Gómez Maqueo Chew<sup>5</sup>, D. R. Anderson<sup>6</sup>, S. C. C. Barros<sup>7</sup>, F. Bouchy<sup>7</sup>, P. Boumis<sup>8</sup>, G. Bruno<sup>7</sup>, A. Collier Cameron<sup>9</sup>, B. Courcol<sup>7</sup>, G. R. Davies<sup>10,11</sup>, F. Faedi<sup>1</sup>, C. Hellier<sup>6</sup>, J. Kirk<sup>1</sup>, K. W. F. Lam<sup>1</sup>, A. Liakos<sup>8</sup>, T. Louden<sup>1</sup>, P. F. L. Maxted<sup>6</sup>, H. P. Osborn<sup>1</sup>, E. Palle<sup>12,13</sup>, J. Prieto Arranz<sup>12,13</sup>, S. Udry<sup>14</sup>, S. R. Walker<sup>1</sup>, R. G. West<sup>1</sup>, P. J. Wheatley<sup>1</sup>

The WASP Consortium consists of representatives from the Universities of Keele, Leicester, The Open University, Queens University Belfast, St Andrews and Warwick, along with the Isaac Newton Group (La Palma) and the Instituto de Astrofísica de Canarias (Tenerife). SuperWASP-North is hosted by the Isaac Newton Group and the Instituto de Astrofísica de Canarias; we gratefully acknowledge their ongoing support and assistance. The SuperWASP cameras are operated with funds available from Consortium Universities and the STFC. The SOPHIE observations were made possible thanks to OPTICON funding allocations 2014A/043 (PI Faedi) and 2014B/029 (PI Gómez Maqueo Chew). YGMC has been partially funded by *Programa UNAM-DGAPA-PAPIIT IA-103215*. This research has made use of NASA's Astrophysics Data System Bibliographic Services.

---

<sup>1</sup>Department of Physics, University of Warwick, Coventry CV4 7AL, UK

<sup>2</sup>Institut d'Astrophysique de Paris, UMR7095 CNRS, Université Pierre & Marie Curie, 98bis boulevard Arago, 75014 Paris, France

<sup>3</sup>Observatoire de Haute-Provence, CNRS, Université d'Aix-Marseille, 04870 Saint-Michel-l'Observatoire, France

<sup>4</sup>ARC, School of Mathematics & Physics, Queen's University Belfast, University Road, Belfast BT7 1NN, UK

<sup>5</sup>Instituto de Astronomía, UNAM, 04510, México, D.F., México

<sup>6</sup>Astrophysics Group, Keele University, Staffordshire ST5 5BG, UK

<sup>7</sup>Aix Marseille Université, CNRS, LAM (Laboratoire d'Astrophysique de Marseille) UMR 7326, 13388, Marseille, France

<sup>8</sup>IAASARS, National Observatory of Athens, GR-15236 Penteli, Greece

<sup>9</sup>SUPA, School of Physics & Astronomy, University of St. Andrews, North Haugh, St. Andrews, Fife KY16 9SS, UK

<sup>10</sup>School of Physics and Astronomy, University of Birmingham, Birmingham, B15 2TT, UK

<sup>11</sup>Stellar Astrophysics Centre (SAC), Department of Physics and Astronomy, Aarhus University, Ny Munkegade 120, DK-8000 Aarhus C, Denmark

<sup>12</sup>Instituto de Astrofísica de Canarias, Via Lactea s/n 38200, La Laguna, Spain

<sup>13</sup>Departamento de Astrofísica, Universidad de La Laguna (ULL), La Laguna, 38205, Tenerife, Spain

<sup>14</sup>Observatoire de Genève, Université de Genève, Chemin des maillettes 51, 1290 Sauverny, Switzerland

# Contents

<b>Declaration of Authorship</b>	<b>i</b>
<b>Abstract</b>	<b>ii</b>
<b>Acknowledgements</b>	<b>iii</b>
<b>Contents</b>	<b>iv</b>
<b>List of Figures</b>	<b>vi</b>
<b>List of Tables</b>	<b>viii</b>
<b>1 Introduction</b>	<b>1</b>
1.1 An introduction to exoplanets . . . . .	1
1.2 Hot Jupiters . . . . .	2
1.2.1 The inflated radius problem . . . . .	2
1.2.2 Tidal interactions between hot Jupiters and their hosts . . . . .	3
<b>2 Methods</b>	<b>5</b>
2.1 Exoplanet detection methods . . . . .	5
2.1.1 Radial Velocity Searches . . . . .	5
2.1.2 Transit Searches . . . . .	7
2.2 The WASP survey . . . . .	8
2.2.1 Finding transit signals in the data . . . . .	8
2.3 Eliminating false positives . . . . .	9
2.3.1 Background eclipsing binaries . . . . .	9
2.3.2 Grazing binary stars . . . . .	10
2.3.3 Planet-sized stars . . . . .	10
2.4 Radial-velocity follow-up . . . . .	11
2.4.1 Bisector spans . . . . .	11
2.4.2 Stellar spectral analysis . . . . .	11
2.5 Follow-up photometry . . . . .	13
2.6 MCMC fitting . . . . .	13
<b>3 Results &amp; Analysis</b>	<b>15</b>

---

3.1	SuperWASP photometry . . . . .	15
3.2	Radial velocity data . . . . .	16
3.3	NITES follow-up photometry . . . . .	19
3.4	Spectral Analysis . . . . .	20
3.4.1	Stellar Age Estimates . . . . .	21
3.5	MCMC System Parameters . . . . .	22
<b>4</b>	<b>Conclusion</b>	<b>25</b>
	<b>Bibliography</b>	<b>27</b>

# List of Figures

1.1	Theoretical mass-radius relation from Zepolsky and Salpeter [1969] for spheres of various chemical elements which are labelled accordingly, with $X=.75$ representing a 3:1 Hydrogen:Helium mix. Jupiter, Saturn, Uranus and Neptune are also plotted. The peak in the mass-radius relation occurs at the theoretical maximum planetary radius, where gravity overcomes electrostatic forces. . . . .	3
1.2	Planetary radii as a function of incident flux, from Demory and Seager [2011]. Before the cut-off point of $\sim 2 \times 10^8 \text{ erg s}^{-1} \text{ cm}^{-2}$ there is a correlation between planet radius and incident stellar flux. The black filled circles are KOI (Kepler Objects of Interest) ranked as planetary candidates, while grey diamonds represent validated Kepler planets. Other giant planets, mostly from ground-based surveys, are shown as red triangles. . . . .	4
2.1	The effect of a planet on the motion of its host star can be detected by measuring the Doppler shift of light received from that star. The barycentre of this system is marked with a cross. . . . .	6
2.2	Orbital motion of 51 Peg from Mayor and Queloz [1995], signalling the first exoplanet found around a sun-like star. . . . .	6
2.3	When a planet's orbit is aligned so that it periodically passes in front of its host star it can be detected by measuring the slight dip in the stellar flux. . . . .	7
2.4	A periodogram from the WASP archive showing the values of $\Delta\chi^2(P)$ plotted against their sampled period. The sharp dip at 1.34 days suggests a strong transit signal of this period. . . . .	9
2.5	Calculating the bisector velocity span of a spectral lines, from Martínez Fiorenzano et al. [2005]. Top panel shows the line bisector as a column of crosses down the middle of the normalised spectral line, with the top and bottom regions labelled. The difference between the average velocity in these two regions is the bisector velocity span. The bottom panel is a re-scaled bisector profile to illustrate the line profile asymmetry. . . . .	12
3.1	Top panel: WASP data phase-folded on a period of 1.40138 days, with over-plotted bins of width $\sim 7$ minutes. Lower panels: binned follow-up photometry from NITES with residuals, bin widths $\sim 3$ minutes, over plotted with the best fitting transiting planet model using the formalism of Mandel and Agol [2002]. . . . .	16
3.2	All SOPHIE radial velocity data, with the best fitting Keplerian model over plotted. The variations in phase with the transit photometry suggest a sub-stellar companion of $\sim 2M_{\text{Jup}}$ . . . . .	19
3.3	CCF bisector span plotted against orbital phase and radial velocity . . . .	19

- 
- 3.4 Output from MCMC chains, showing correlations between system parameters. Strong correlations can be seen between highly degenerate parameters in the transit and Keplerian models, such as  $M_*$  and  $M_p$ , or  $R_*$  and  $R_p$ . . . . . 24
- 4.1 Planetary radii as a function of incident flux, from Demory and Seager [2011]. Same as Figure 1.2, with the inflated planet WASP-135b added as a green square. Before the cut-off point of  $\sim 2 \times 10^8 \text{ erg s}^{-1} \text{ cm}^{-2}$  there is a correlation between planet radius and incident stellar flux. . . . . 26

# List of Tables

3.1	Radial velocity measurements of WASP-135 from SOPHIE, with bisector spans from spectral line profiles. . . . .	18
3.2	Stellar parameters of WASP-135 from spectroscopic analysis. . . . .	21
3.3	Stellar age estimates for WASP-135. . . . .	22
3.4	MCMC system parameters for WASP-135 . . . . .	23

# Chapter 1

## Introduction

### 1.1 An introduction to exoplanets

The idea of alien worlds orbiting other stars has been inspiring humans for hundreds of years. Galvanised by the novel suggestion by Copernicus that the Earth is in orbit around the Sun, in 1584 Giordano Bruno put forward the idea that the stars in the night sky were suns themselves, with their own planets, perhaps even hosting their own forms of life [Bruno, 1584]. We call these worlds exoplanets. It wasn't until 1995 that the first exoplanet orbiting a Sun-like star was actually discovered, by Mayor and Queloz [1995], and since then our understanding of exoplanets has advanced at a remarkable pace. The search for earth-like, habitable planets and signs of extra-solar life has motivated unprecedented leaps in our understanding of exoplanets, and our place in the Universe.

For example, we have learnt of the astonishing diversity of exoplanets, which have a much larger range of masses, sizes, temperatures, compositions and stellar environments than was previously thought possible. Additionally, in the short period of time since the first exoplanet discovery, estimates of the occurrence rate of earth-like planets in the Milky Way (e.g. Petigura et al. [2013], Dressing and Charbonneau [2015]) have been made, which is an important step in our understanding of the prevalence of extra-terrestrial life. We are even moving into the era of detailed atmospheric characterisation for some exoplanets. Molecules (e.g. Charbonneau et al. [2002]), clouds (e.g. Sing et al. [2015]) and spatially resolved winds (e.g. Louden and Wheatley [2015]) have been detected in the atmospheres of exoplanets.

Many new avenues of exoplanet research have opened, and many exciting questions about the exoplanet population have been raised. One class of exoplanets in particular has raised more questions than most - a class called the hot Jupiters. This work covers the discovery of WASP-135b [Spake et al., 2015], a new planet of this type.

## 1.2 Hot Jupiters

The first exoplanet found orbiting a Sun-like star, 51 Peg b, was a hot Jupiter [Mayor and Queloz, 1995]. Hot Jupiters are gas giants that orbit so close to their host stars that some have periods as short as 19 hours [Hebb et al., 2010]. They were a shock to discover, because it was thought that gas giants could not form so close to stars [Pollack et al., 1996]. They are exotic planets; unlike anything in the Solar System and intrinsically rare in our Galaxy. Two of the many mysteries surrounding hot Jupiters are discussed below.

### 1.2.1 The inflated radius problem

Many hot Jupiters have larger radii than was predicted by planetary evolution models, and the reason for this radius anomaly is not yet fully understood. Reviews of this phenomenon can be found in Fortney and Nettelmann [2010] and Baraffe et al. [2010]. Essentially, the more massive a planet, the larger the force of gravity felt by its outer layers. This force prevents the radius becoming much larger for gas giants of considerably higher mass. For extremely high mass planets the gravity is strong enough to overcome electrostatic forces, and electron degeneracy becomes the significant opposing force. At this point the radius stops increasing with mass. This turnaround can be seen in Figure 1.1, which shows the theoretical mass-radius relationships for spheres of various chemical elements, and their expected maximum radii.

The fact that a large number of hot Jupiters appear to have inflated radii suggests that there is some underlying physics that has not been understood. It has been proposed that the high levels of incident flux received by these planets which orbit so close to their stars may be the cause of this radius anomaly. Indeed there is growing evidence of a positive correlation between levels of incident stellar flux and giant planet radius, for example in Enoch et al. [2011] and Weiss et al. [2013]. In a study of 115 *Kepler* giant planet candidates, Demory and Seager [2011] find an increase in planet radii with increased stellar irradiation, for highly irradiated planets receiving fluxes of more than  $\sim 2 \times 10^8$  erg s<sup>-1</sup> cm<sup>-2</sup>. This can be seen in Figure 1.2. However, the exact mechanisms which transport the energy into the interior of planets remain disputed. Proposed theories include Ohmic heating [Batygin and Stevenson, 2010] and kinetic heating [Guillot and Showman, 2002], among others.

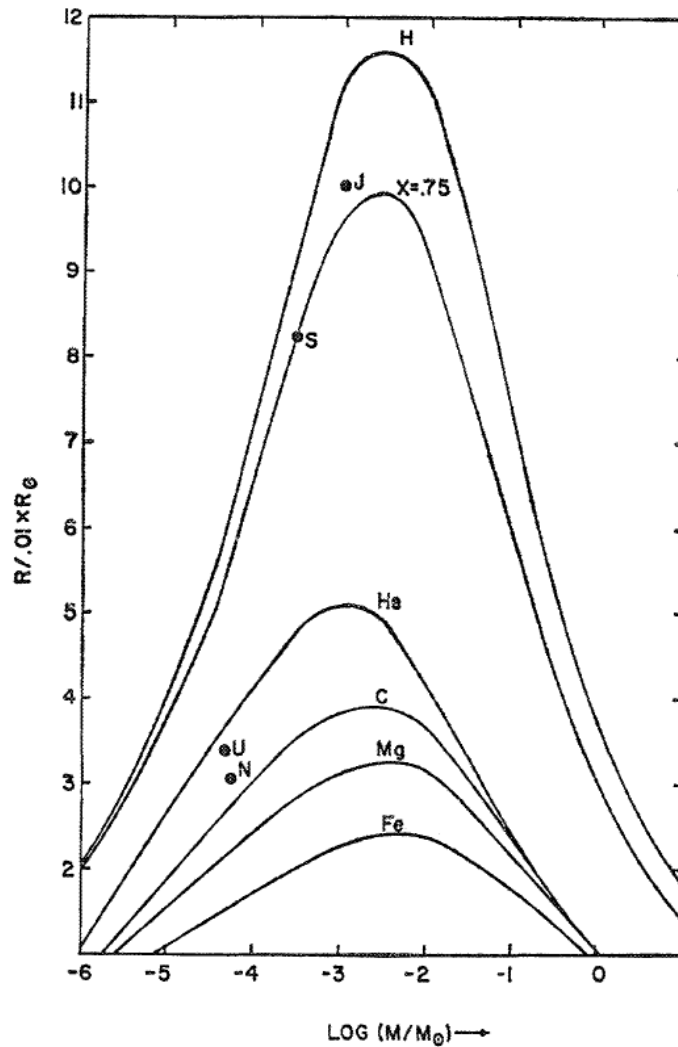


**Figure 1.1:** Theoretical mass-radius relation from Zapolsky and Salpeter [1969] for spheres of various chemical elements which are labelled accordingly, with  $X=.75$  representing a 3:1 Hydrogen:Helium mix. Jupiter, Saturn, Uranus and Neptune are also plotted. The peak in the mass-radius relation occurs at the theoretical maximum planetary radius, where gravity overcomes electrostatic forces.

### 1.2.2 Tidal interactions between hot Jupiters and their hosts

Generally, as a star ages its rotation rate will slow. Gyrochronology uses this phenomenon to calculate the ages of stars with a measured rotation rate. Some, such as Lanza [2010], suggest that for hot Jupiter host stars, a gyrochronological age significantly younger than age estimates found by other means is evidence of tidal 'spin-up'. This is a possible transfer of angular momentum from the massive, close-in planet to the star. If real, this process would hinder the normal stellar spin-down mechanisms, leaving the star rotating faster, and appearing younger than expected from gyrochronological models. Some hints of this effect have been seen, for example Pont [2009] finds empirical

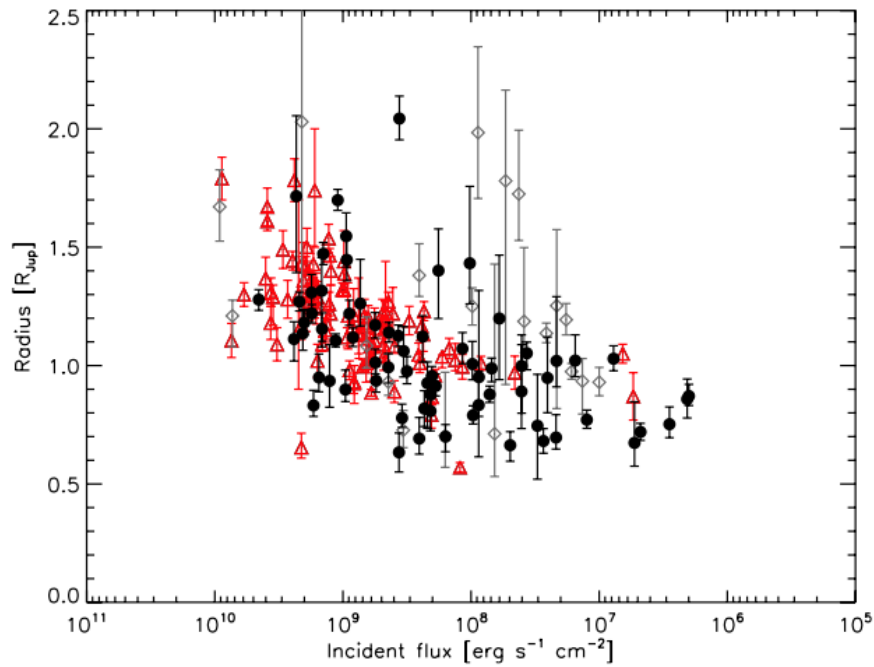


**Figure 1.2:** Planetary radii as a function of incident flux, from Demory and Seager [2011]. Before the cut-off point of  $\sim 2 \times 10^8 \text{ erg s}^{-1} \text{cm}^{-2}$  there is a correlation between planet radius and incident stellar flux. The black filled circles are KOI (Kepler Objects of Interest) ranked as planetary candidates, while grey diamonds represent validated Kepler planets. Other giant planets, mostly from ground-based surveys, are shown as red triangles.

evidence of faster rotation in stars with closer and more massive planets, and Brown [2014] and Maxted et al. [2015] both find a tendency for planet hosting stars to have younger gyrochronological ages than their isochronal age estimates.

# Chapter 2

## Methods

### 2.1 Exoplanet detection methods

Detecting any exoplanet directly is extremely difficult, since interstellar distances are so great, and planets tend to emit almost negligible radiation compared to their host stars. However, it has been possible to directly image a few exoplanets (for example 2M1207b Chauvin et al. [2004], and the multi-planet HR 8799 system Marois et al. [2008]), but this is only feasible for young, massive planets in extremely wide orbits.

To date, most exoplanets discovered have been found using indirect methods. The two most successful - radial velocity and transit searches - are discussed below.

#### 2.1.1 Radial Velocity Searches

All bodies in a planetary system orbit the common centre of mass, or barycentre, as shown in Figure 2.1. Since the star of a typical system will make up most of the mass, the barycentre tends to be close to the centre of the star. However, it is possible to detect the relatively small motion of the star about the barycentre - called the reflex orbit - and thus indirectly learn of the planets in the system.

It is possible to accurately measure the radial velocity (the component of its velocity directly towards or away from the observer) of a star by the Doppler shift of its emitted spectrum<sup>1</sup>. Planets are detected by measuring periodic, back-and-forward 'wobbles' of the star. This was the method used to detect 51 Peg b, and its orbital motion can

---

<sup>1</sup>In theory it is also possible to directly image the reflex orbit with extremely precise measurements of the star's position (called astrometry) over time. No planets have been discovered with this method yet, but ESA's new *Gaia* mission [Lindgren and Perryman, 1996] is expected to find thousands to tens of thousands of exoplanets in this way over its five-year mission [Perryman et al., 2014].

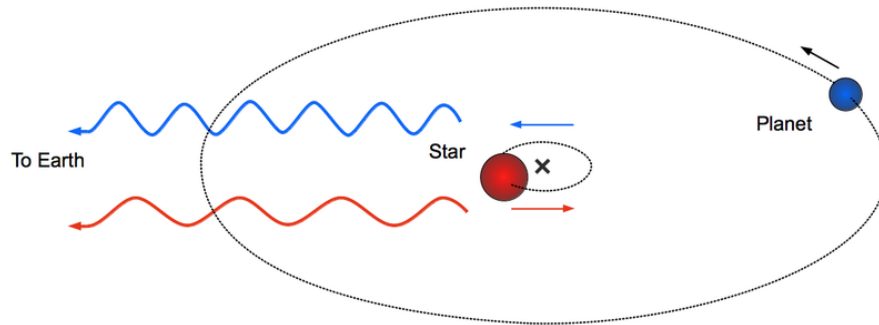


**Figure 2.1:** The effect of a planet on the motion of its host star can be detected by measuring the Doppler shift of light received from that star. The barycentre of this system is marked with a cross.

be seen in the radial velocity measurements in Figure 2.2. Hot Jupiters like 51 Peg b are suited to this detection technique because their large masses and close orbits cause larger changes in the radial velocity of the star. If the mass of the star is known then the minimum mass of the planet can be measured via the amplitude of the variation. Knowing the orbital inclination of the system allows us to remove the inclination-velocity amplitude degeneracy. For fortunately-aligned systems this can be measured with the transit technique (discussed below).

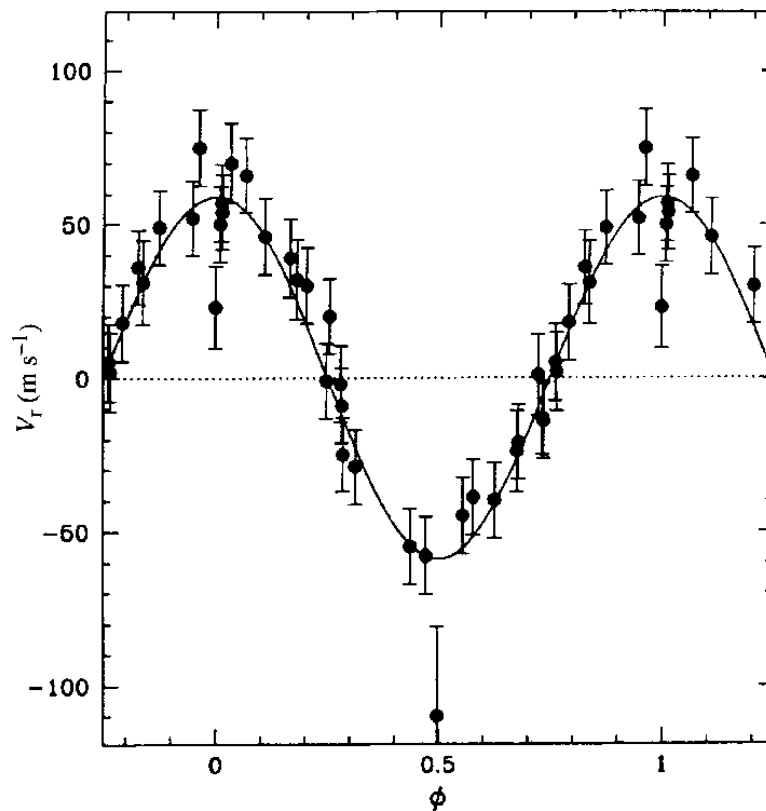


**Figure 2.2:** Orbital motion of 51 Peg from Mayor and Queloz [1995], signalling the first exoplanet found around a sun-like star.

### 2.1.2 Transit Searches

Assuming all planetary systems are oriented randomly, some of them are aligned so that a planet passes in front of its host star each orbit, blocking out some of the starlight, as seen in Figure 2.3. By measuring the brightness of stars over long periods of time and searching for these periodic transits, thousands of planets and planet candidates have been found to date<sup>2</sup>. Notable ground-based transit surveys include the Super-WASP [Pollacco et al., 2006] and HATNet [Bakos et al., 2004] surveys, with 113 and 60 confirmed planets respectively. The space-based *Kepler* [Borucki et al., 2010] and K2 [Howell et al., 2014] surveys have detected nearly 2500 confirmed planets between them (as of September 2016).

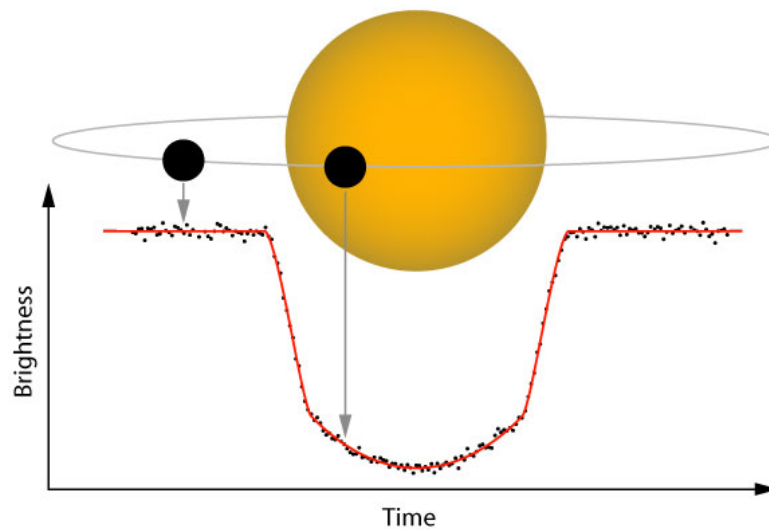


**Figure 2.3:** When a planet’s orbit is aligned so that it periodically passes in front of its host star it can be detected by measuring the slight dip in the stellar flux.

Transiting exoplanets are extremely important as they remain the only ones for which accurate measurements of the planet radius can be made. This is because the ratio of the depth of the transit signal is proportional to the square of the planet-to-star radius ratio:

$$\frac{\Delta F}{F} = \frac{R_P^2}{R_*^2}$$

where  $F$  is the flux measured from the star, and  $\Delta F$  is the change in flux during transit, and  $R_P$  and  $R_*$  are the planet and stellar radius respectively. Knowing the radius of an exoplanet is extremely important, as it is necessary to calculate the bulk density, which is a fundamental planetary property. Transiting exoplanets around bright stars are also excellent targets for atmospheric characterisation.

<sup>2</sup>[exoplanetarchive.ipac.caltech.edu/](http://exoplanetarchive.ipac.caltech.edu/)

## 2.2 The WASP survey

WASP-135b was found with the WASP transit survey, which consists of two similar observatories of small, wide-field cameras which continually monitor millions of the brightest stars across the entire sky. SuperWASP-North is at the Observatorio del Roque de los Muchachos on La Palma, Spain, and covers the northern hemisphere of the sky. It was with this observatory that WASP-135b was discovered. The instrument consists of 8 cameras, with Canon 200-mm f/1.8 lenses and  $2048 \times 2048$  e2V CCD detectors, each with a field-of-view of  $7.8^\circ \times 7.8^\circ$  and a plate scale (the amount of sky covered by each pixel, usually in arcseconds per pixel) of  $13''.7 \text{ pixel}^{-1}$ . The WASP survey and data reduction procedures are discussed in detail in Pollacco et al. [2006].

### 2.2.1 Finding transit signals in the data

WASP has been measuring the brightness of tens of millions of stars since 2006. This data is stored on the online WASP archive for analysis. A typical star may have tens of thousands of measurements spanning nearly a decade. This data is automatically searched for periodic transit signals via the Box Least Squares (BLS) fit method, described in Kovács et al. [2002]. In essence, the data is fitted with a simple, box-shaped model, with two brightness levels - one for out of transit and a slightly lower, in-transit level. In reality the shape of the transit lightcurve is more complex (as seen in Figure 2.3), but the noise in WASP data is greater than this difference. Every realistic period, transit depth and duration is then modelled and compared with the data. The 'goodness of fit' of each model to the data is then measured, by calculating the quantity called  $\chi^2$ , given by

$$\chi^2 = \sum_i \left( \frac{x_i - \mu_i}{\sigma_i} \right)^2$$

where  $x_i$  are the measured brightness values,  $\mu_i$  are the corresponding model values, and  $\sigma_i$  are the errors on the measured values. The minimum  $\chi^2$  value for each period,  $\chi_{min}^2(P)$ , is then found, and compared with the  $\chi_{constant}^2$  of a model consisting of a flat line of constant brightness. For each period, the following quantity is calculated:

$$\Delta\chi^2(P) = \chi_{min}^2(P) - \chi_{constant}^2$$

and plotted against the period,  $P$ . An example of this type of graph, called a periodogram, can be seen in Figure 2.4. Sharp dips like the one seen at 1.34 days indicate a strong periodic transit signal in the data, since the model with that period fits the data much better than a flat line model.

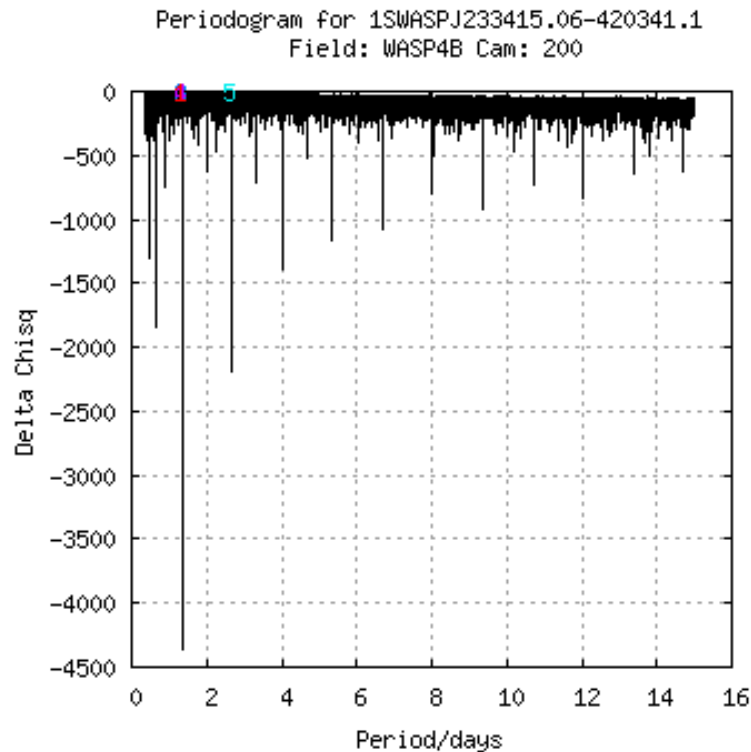


**Figure 2.4:** A periodogram from the WASP archive showing the values of  $\Delta\chi^2(P)$  plotted against their sampled period. The sharp dip at 1.34 days suggests a strong transit signal of this period.

## 2.3 Eliminating false positives

Once a transit signal has been detected, there is much to do before it is possible to say definitively that the signal is due to an exoplanet. There are many false positives that can mimic a transiting exoplanet, and indeed most of the detected signals from the WASP survey are due to other astrophysical phenomena, like eclipsing binary stars. Thus there are many possibilities to eliminate before one can confirm the discovery of a transiting exoplanet, and these are discussed below.

### 2.3.1 Background eclipsing binaries

A system of two gravitationally bound stars orbiting each other is called a binary system, and some are aligned so that they eclipse each other every orbit. Because of the much larger radii of stars compared to planets these make periodic dips far larger than planetary transits (which have a maximum depth of about 2% depending on the host star), so they tend to be very easy to distinguish from planetary sized companions. However like most transit surveys, WASP uses CCDs with a large plate scale, which means there

is often more than one detectably bright source per pixel. Occasionally a bright star may be blended with a fainter, background eclipsing binary system, diluting the binary eclipses leading to similarly sized dips in brightness to a transiting planet. These may be flagged as planet candidates in the initial transit search.

Background eclipsing binaries may be eliminated in several ways. Firstly, if the mass (and thus radius and luminosity) of each star in the binary system is unequal, the 'transit' depths will have alternating larger and smaller depths as the stars of alternating brightness are eclipsed. These alternating depths can sometimes be seen in the survey data<sup>3</sup>. Secondly, one can image the source with an instrument with a higher plate-scale, in order to resolve any blended sources. Thirdly, eclipsing binary systems should have V-shaped lightcurves, whereas planetary transit lightcurves should be fairly flat-bottomed as the entire planet passes in front of the stellar disk. Observing a single transit with high enough time resolution and signal-to-noise ratio so that the shape is clear should be enough to distinguish between the two scenarios.

### 2.3.2 Grazing binary stars

If a binary system is aligned so that the eclipses are only 'grazing' - that is, only the outer limb of one star crosses the disk of the other - the depth of the eclipse may be small enough to mimic a planetary transit. A high-quality transit lightcurve is therefore necessary in this case, in order to spot the tell-tale V-shaped signal from a grazing binary system.

### 2.3.3 Planet-sized stars

White dwarfs, which are approximately Earth-sized, and brown dwarf stars, which are approximately Jupiter-sized, can mimic exoplanets in transit searches, since their lightcurves can be indistinguishable. These stellar mimics are impossible to eliminate without a measurement of the mass of the transiting object, by observing the changing radial velocity. Therefore a transiting planet will remain a candidate until its planetary mass has been confirmed. As an example, the transiting object EPIC201702477b found with *Kepler* was initially validated as a planet candidate [Foreman-Mackey et al., 2015], before radial velocity follow-up measurements revealed that its mass ( $66.9 \pm 1.7 M_J$ ) falls in the brown dwarf range [Bayliss et al., 2016]. Four more transiting brown dwarfs have been discovered with *Kepler*, and three with the space-based CoRoT mission. From the ground only two transiting brown dwarfs have been discovered to date - WASP-30b

---

<sup>3</sup>However, if the stars in the binary system are of equal mass (and radius and luminosity), the alternating eclipses will be identical, making them very similar to planetary transit signals.

[Anderson et al., 2011] and KELT-1 b [Siverd et al., 2012]. A transiting object with a radius consistent with an Earth-sized planet was found in the *Kepler* lightcurves, but was found to be a white dwarf. Interestingly, the stellar mass of the transiting companion was confirmed using gravitational lensing [Kruse and Agol, 2014].

## 2.4 Radial-velocity follow-up

Once a suitable candidate has been identified from the WASP survey, and eclipsing binary star mimics have been ruled out, preliminary spectroscopic measurements of the host star candidate can be made. First, a single spectrum of the target star is observed. This is to check the possibility that the target star is a giant. A 2% transit on a sun-like star could be due to a Jupiter-sized planet, but if the star is a giant, the same sized signal is likely due to a much bigger object. If the star appears to be on the main sequence more spectra are then taken at various different points throughout the period detected from the transit search. These are used to look for radial velocity variations in phase with the period, of the order of 500 km/s or less, which correspond to a companion of approximately planetary mass.

### 2.4.1 Bisector spans

The radial velocity of the target star is found by measuring the Doppler shift of thousands of spectral lines in a single spectrum. These spectral features are caused by physical phenomena in the atmosphere of the star. Activity in the stellar atmosphere changes the profile (shape) of spectral lines, and may also mimic radial velocity variations. It is therefore necessary to rule out stellar activity as the source of apparent radial velocity variations. This is done by looking for correlations between the measured radial velocity values and any asymmetry in the spectral line profiles. The asymmetry of a spectral line profile can be measured using the bisector velocity span (BVS) [Toner and Gray, 1988]. The calculation of this quantity is illustrated in Figure 2.5. If there is no correlation between the BVS and the measured radial velocity values, it is likely that the variations are due to movement of the star and not stellar activity.

### 2.4.2 Stellar spectral analysis

In order to characterise the physical properties of an exoplanet, it is essential to characterise the physical properties of its host star. If the radius of a star is not well constrained, it is impossible to accurately infer the radius of a transiting planet. Likewise if the mass

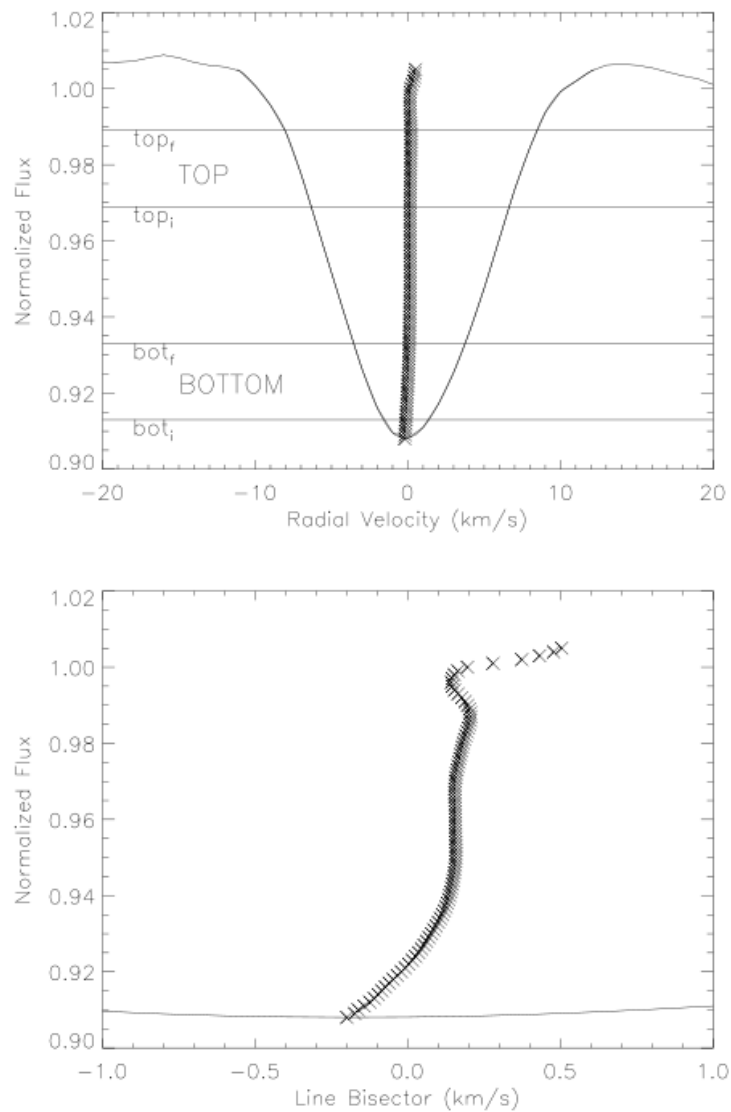


**Figure 2.5:** Calculating the bisector velocity span of a spectral lines, from Martínez Fiorenzano et al. [2005]. Top panel shows the line bisector as a column of crosses down the middle of the normalised spectral line, with the top and bottom regions labelled. The difference between the average velocity in these two regions is the bisector velocity span. The bottom panel is a re-scaled bisector profile to illustrate the line profile asymmetry.

of a star is unknown, Kepler’s third law cannot be used to calculate the planetary mass. Many physical parameters of a star may be determined by studying features in its spectrum (although the stellar density can actually be deduced from the shape of a transit lightcurve, as explained in Seager and Mallén-Ornelas, 2003). For example, the effective temperature of a star,  $T_{\text{eff}}$ , can be calculated by measuring the excitation balance of different ions of Iron. The relative strengths of absorption lines in the spectrum from the

excitation of different ions will suggest their relative abundances, and from this an effective temperature can be inferred (higher temperatures will lead to stronger ionisations). Properties such as  $T_{\text{eff}}$  that can be directly measured from the spectrum are combined with stellar models to gain accurate estimates for other parameters like stellar mass and radius. Comparing the stellar parameter values determined from different methods - from the transit lightcurve shape and from the analysis of the combined spectra taken from the radial velocity measurements - can be extremely useful.

## 2.5 Follow-up photometry

WASP is a wide-field survey. In order to achieve a large field of view, the instruments employ small apertures. This means that relatively few photons per star are detected on its CCD arrays, compared with larger telescopes. For this reason, WASP lightcurves are dominated by a large photon noise. Although a periodic transit signal for a gas-giant planet may be detected in the data, its shape will not be well defined. Because of this, it is usually necessary to dedicate at least one night with a larger telescope to observe a full planetary transit. This temporally-resolved light curve can be used to better determine the transit shape, and measure important quantities like the transit depth and duration to a higher degree of accuracy.

## 2.6 MCMC fitting

The crux of the method of finding a new exoplanet with SuperWASP is fitting a model of the star-planet system to all observations simultaneously, and retrieving the physical parameters (like planet mass and orbital distance) which fit the data best. In Section 2.2.1 the basic principles of chi-squared minimisation were discussed, which is a useful method for finding best-fitting models for a data set. Markov chain Monte Carlo (MCMC) methods are a set of Bayesian algorithms which can use chi-squared minimisation to find best fitting parameters and their errors in a statistically robust way. They are used very commonly in astronomy and other sciences. In this case a Keplerian model is fitted to the radial velocity data whilst a Mandel and Agol [2002] analytical model for the transit lightcurves is simultaneously fit to the photometric data, in order to find the system parameters such as planetary mass, radius and orbital distance.

MCMC methods generate a chain of states in the parameter space. The decision of whether to take the next jump in the chain is based on a set of rules which ensure the convergence of the chain to the Posterior Probability Distribution. The following steps describe the basic method (from Ford [2005]):

- 
- The chain is initialised with a value for each of the parameters,  $x_n$ . This is the  $n = 0$ th step of the chain.
  - A trial state ( $x'$ ) is generated according to a transition kernel,  $q(x'|x_n)$ , such as a Gaussian function centred on  $x_n$
  - The models (in this case the Keplerian and Mandel & Agol models) are evaluated at this trial state,  $f_{model}(x')$ , along with the associated  $\chi^2(x')$
  - The probability of the transition from the  $n$ th state to the trial state is calculated, which is proportional to  $\exp(-\frac{1}{2}[\chi^2(x') - \chi^2(x_n)])$
  - A random number is drawn from a uniform distribution between 0 and 1
  - If this random number is below the transition probability then the trial step is taken, i.e.  $x_{n+1} = x'$ . If not, the trial step is rejected and  $x_{n+1} = x_n$
  - The process is repeated with  $n = n + 1$  until the chain has reached its limit (chains of the order of 10,000 steps are common)

## Chapter 3

# Results & Analysis

### 3.1 SuperWASP photometry

WASP-135 (1SWASPJ174908.40+295244.9) is a G5V star with  $V = 13.28$  and  $B - V = 0.97$  [Zacharias et al., 2013]. It was observed by SuperWASP-N at the Observatorio del Roque de los Muchachos on La Palma, Spain from 2004 May 05 to 2010 August 24, and 34699 observations were made in total.

An exoplanet candidate with a period of 1.401 days was identified using transit detection methods described in Collier Cameron et al. [2006] and Pollacco et al. [2008]. The top panel of Figure 3.1 shows the WASP photometry, folded on the best-fitting orbital period. Additional planet candidates were searched for in the WASP data, by subtracting a transit model due to the known candidate from the data, then searching the residual light curves for additional periodic transit events with periods up to 40 days but none were found. This method is described in Smith et al. [2009]. Although the WASP data spans over 6.5 years, systematic noise limits the search for periodicity on very long timescales. The WASP data was also searched for photometric variability as could be caused by magnetic activity and stellar rotation, as described in Maxted et al. [2011]. No significant signals were found above the 3-mmag level.

Before analysis, the timings for all data including WASP photometry were converted to  $\text{BJD}_{\text{TDB}}$  using the method of Eastman et al. [2010].

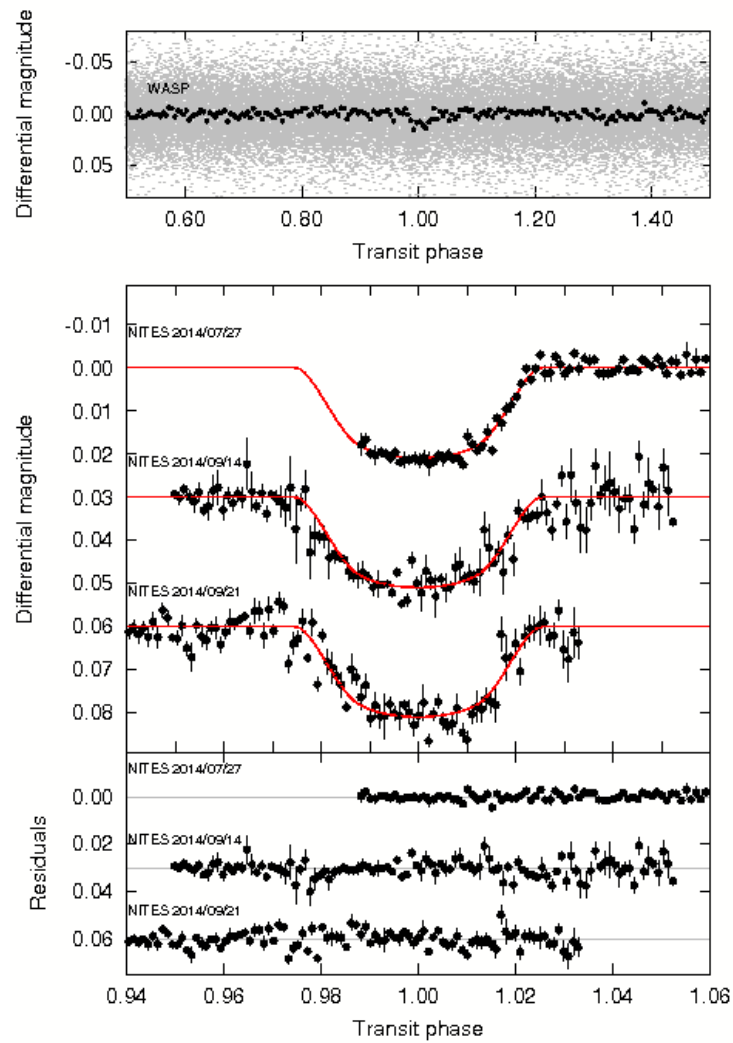


**Figure 3.1:** Top panel: WASP data phase-folded on a period of 1.40138 days, with over-plotted bins of width  $\sim 7$  minutes. Lower panels: binned follow-up photometry from NITES with residuals, bin widths  $\sim 3$  minutes, over plotted with the best fitting transiting planet model using the formalism of Mandel and Agol [2002].

## 3.2 Radial velocity data

Spectroscopic follow-up of WASP 135 was conducted with the SOPHIE spectrograph mounted on the 1.93m telescope of the Observatoire de Haute-Provence, France<sup>1</sup>. More details about the instrument can be found in Bouchy et al. [2009].

Measurements were made of the radial velocity of the star at many points throughout the proposed orbital phase. In the case of a planetary system, the signal should describe a Keplerian motion of the planet host around the system's centre of mass, yielding the

<sup>1</sup>These observations were made mainly by G. Hébrard

minimum planetary mass, period, semi-major axis, orbital eccentricity and argument of periapsis. The radial velocity measurements also allow us to discard astrophysical false positives such as blended stellar binaries.

SOPHIE was used in High-Efficiency mode (HE) with a resolving power  $R = 40000$  to increase the throughput for this faint target. The typical exposure times were 30 minutes, but they were slightly adjusted as a function of the weather conditions to keep the signal-to-noise ratio at  $\sim 30$ . The spectra were extracted using the SOPHIE pipeline, and the radial velocities were measured from the weighted cross-correlation with a numerical mask [Baranne et al., 1996, Pepe et al., 2002]. We adjusted the number of spectral orders used in the cross-correlation to reduce the dispersion of the measurements. Indeed, some spectral domains are noisy (especially in the blue part of the spectra), so using them degrades the accuracy of the radial velocity measurement.

The error bars on the radial velocities were computed from the cross-correlation function (CCF) using the method presented by Boisse et al. [2010]. We estimated the moonlight contamination using the second SOPHIE fiber aperture, which is targeted on the sky while the first aperture points toward the target. We found RV shifts due to Moonlight contamination below  $10 \text{ ms}^{-1}$  in all cases, and concluded that there is no significant Moon pollution in our data. Radial velocities measured using different stellar masks (F0, G2, K0, or K5) produce variations with similar amplitudes, so there is no evidence that their variations could be explained by blend scenarios caused by stars of different spectral types.

In total 21 observations were made between 2014 May 30 and 2014 October 02. These are reported in Table 3.1 and displayed in Figure 3.2, together with the Keplerian fit and the residuals. They show variations in phase with the SuperWASP transit ephemeris and with a semi-amplitude of  $346 \pm 35 \text{ ms}^{-1}$ , implying a companion of  $\sim 2M_{\text{Jup}}$ .

The bisector spans as defined by Toner and Gray [1988] were measured, and applied to the cross-correlation function as in Queloz et al. [2001]. They show neither variations nor trends as a function of radial velocity or orbital phase (Fig. 3.3). Additionally, the RMS of the bisector spans is  $0.05 \text{ kms}^{-1}$ , which is of the order of the radial velocity errors. This reinforces the conclusion that the radial-velocity variations are not caused by spectral-line profile changes attributable to blends or stellar activity.

Two radial velocity measurements were not included in the final analysis and hence do not appear in the figure, although they are included in Table 3.1 for completeness. One (BJD = 2456923.4) was particularly inaccurate due to poor weather conditions. The other (BJD = 2456813.4) is an outlier, and is off by about 100 m/s from the Keplerian model. We looked for possible causes of this shift, including cosmic rays on the detector,

abnormally high drift seen in the wavelength calibration, concern with the CCD reading mode, standard stars observed at the same epoch, sporadic stellar activity events linked to CaII chromospheric emission; we found nothing abnormal. However, a more careful inspection of the CCF shows a small deformation of its profile; it is also seen to have a bisector value slightly lower than values at other epochs. Even if the cause of the CCF deformation is not well understood, it explains the abnormal radial velocity at this epoch. This reinforces its interpretation as an instrumental outlier instead of a signature of an additional companion in the system, in agreement with the fact that other RV measurements secured at similar epochs or similar orbital phase do not show such shifts from the 1-planet Keplerian model.

We thus concluded that our target harbours a transiting giant planet, which we designate WASP-135b hereafter.

**Table 3.1:** Radial velocity measurements of WASP-135 from SOPHIE, with bisector spans from spectral line profiles.

BJD −245000	RV (kms <sup>−1</sup> )	$\sigma_{RV}$ (kms <sup>−1</sup> )	BS (kms <sup>−1</sup> )
56808.4537	−32.017	0.013	0.002
56809.3954	−32.678	0.010	0.022
56810.4489	−32.488	0.011	−0.016
56811.4723	−32.010	0.009	0.052
56812.4370	−32.359	0.019	−0.064
56813.4209 <sup>a</sup>	−32.535	0.015	−0.163
56814.3886	−32.102	0.010	−0.008
56828.4083	−32.137	0.009	−0.000
56829.4019	−32.115	0.010	−0.022
56830.4209	−32.651	0.009	0.042
56856.3802	−32.040	0.010	−0.009
56858.3932	−32.653	0.030	0.177
56868.4157	−32.439	0.014	−0.036
56870.3629	−32.052	0.009	0.006
56897.4126	−32.532	0.022	0.004
56899.3859	−32.246	0.008	−0.015
56900.3450	−32.663	0.008	0.035
56922.3090	−32.128	0.008	0.003
56923.4023 <sup>b</sup>	−32.143	0.063	−0.338
56932.2772	−32.358	0.010	0.014
56933.2939	−31.987	0.010	−0.053

**Notes:** *a*: this measurement was a significant outlier for unknown reasons *b*: poor weather conditions meant that this measurement was particularly inaccurate. Neither were used in the MCMC analysis.

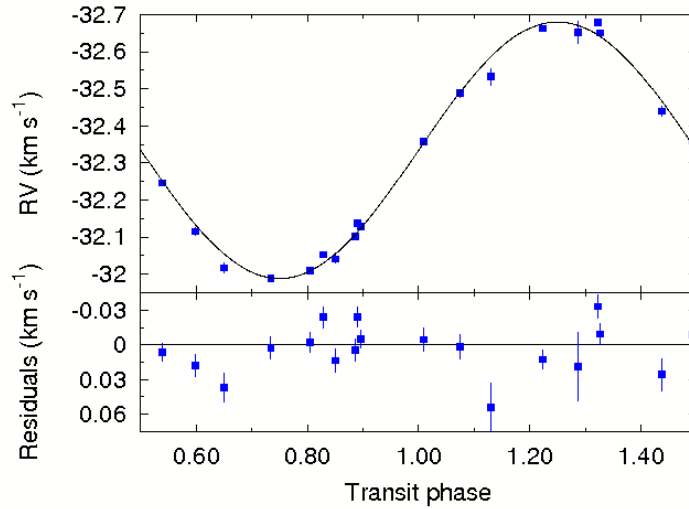


**Figure 3.2:** All SOPHIE radial velocity data, with the best fitting Keplerian model over plotted. The variations in phase with the transit photometry suggest a sub-stellar companion of  $\sim 2M_{\text{Jup}}$ .

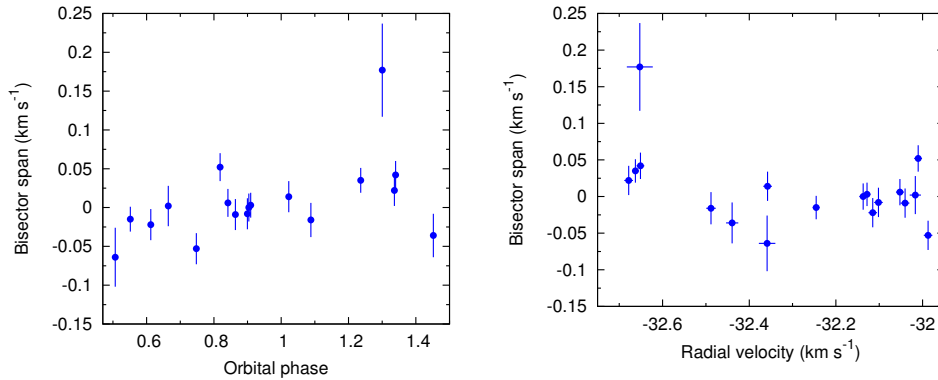


**Figure 3.3:** CCF bisector span plotted against orbital phase and radial velocity

### 3.3 NITES follow-up photometry

Three nights of follow-up observations were carried out with the Near Infra-red Transiting ExoplanetS (NITES) telescope on 2014 July 27, 2014 September 21 and 2014 September 28<sup>2</sup>. NITES is a 0.4m, f/10 Meade telescope located at the Observatorio del Roque de los Muchachos on La Palma, equipped with a camera containing a  $1024 \times 1024$  pixel CCD manufactured by e2v, and no filter. The field of view of the instrument is  $11.3' \times 11.3'$  and it has a plate scale of  $0.66'' \text{ pixel}^{-1}$ . Autoguiding corrections are calculated directly from the science images using the DONUTS algorithm described in McCormac et al. [2013], which allows autoguiding on defocussed target stars. NITES is described in more detail in McCormac et al. [2014].

<sup>2</sup>The first two nights were completed by J. McCormac, and the third was completed by myself and J. McCormac

A clear transit was observed in each of the 3 follow-up nights, however data acquisition began after ingress on 2014 July 07. The middle panel of Figure 3.1 shows the three lightcurves from NITES, in bins approximately 3 minutes wide. The residuals are shown in the bottom panel. Although the beginning of some of the observations were taken at higher airmass (and consequently show larger scatter), with the simultaneous analysis of all three light curves we are able to constrain the start time and shape of the ingress.

The smaller plate scale of the NITES instrument showed the presence of a brighter star on the edge of the large aperture used in the WASP photometry, and 6 fainter sources inside the aperture. This dilution meant that the transit depth in the WASP data was smaller than that found from NITES, by a factor of 2.7. Because of this, the WASP data was used to constrain the ephemeris timing only and not the transit depth. This is discussed further in Section 3.5.

Standard data reduction was performed using PyRAF and the routines in IRAF, and DAOPHOT [Stetson, 1987] was used for aperture photometry using 6 comparison stars. Since the stars were defocussed initial apertures were placed manually, then shifted for each science image using the DONUTS routine [McCormac et al., 2013].

### 3.4 Spectral Analysis

The individual SOPHIE spectra of WASP-135 were co-added to produce a single spectrum with a S/N of around 50 at a wavelength of 5500 Å. The standard pipeline reduction products were used in the analysis. The analysis was performed using the methods given in Doyle et al. [2013]<sup>3</sup>. The effective temperature ( $T_{\text{eff}}$ ) was determined from the excitation balance of the Fe I lines. The Na I D lines and the ionisation balance of Fe I and Fe II were used as surface gravity ( $\log g$ ) diagnostics. The parameters obtained from the analysis are listed in Table 3.2. The iron abundance was determined from equivalent width measurements of several unblended lines. A value for microturbulence ( $\xi_t$ ) was determined from Fe I using the method of Magain [1984]. The quoted error estimates include that given by the uncertainties in  $T_{\text{eff}}$  and  $\log g$ , as well as the scatter due to measurement and atomic data uncertainties. Interstellar Na D lines are present in the spectra with equivalent widths of  $\sim 0.06\text{\AA}$ , indicating an extinction of  $E(B - V) = 0.017 \pm 0.003$  using the calibration of Munari and Zwitter [1997]. Emission is detected in the Ca II H and K lines; however, for a star of this magnitude the SOPHIE spectra are not good enough to estimate a reliable activity index.

<sup>3</sup>This analysis was completed by A. P. Doyle

The projected stellar rotation velocity ( $v \sin i$ ) of  $4.67 \pm 0.89 \text{ km s}^{-1}$  was determined by fitting the profiles of several unblended Fe I lines. This agrees with the  $v \sin i$  value of  $4 \pm 1 \text{ km s}^{-1}$  obtained from the CCF using the calibration by Boisse et al. [2010]. A value for macroturbulence ( $v_{\text{mac}}$ ) of  $2.80 \pm 0.73 \text{ km s}^{-1}$  was determined from the calibration of Doyle et al. [2014]. An instrumental FWHM of  $0.15 \pm 0.01 \text{ \AA}$  was determined from the telluric lines around  $6300 \text{ \AA}$ .

**Table 3.2:** Stellar parameters of WASP-135 from spectroscopic analysis.

Parameter	Value
RA	$17^h 49^m 08^s.4$
DEC	$+29^\circ 52' 45.0''$
V (mag)	13.28
B (mag)	14.251
J (mag)	11.581
K (mag)	11.037
$T_{\text{eff}}$	$5680 \pm 60 \text{ K}$
$\log g$	$4.50 \pm 0.10$
$v \sin i$	$4.67 \pm 0.89 \text{ km s}^{-1}$
$v_{\text{mac}}$	$2.80 \pm 0.73 \text{ km s}^{-1}$
$\xi_t$	$0.70 \pm 0.10 \text{ km s}^{-1}$
[Fe/H]	$0.02 \pm 0.13$
$\log A(\text{Li})$	$2.01 \pm 0.06$
Mass	$1.01 \pm 0.07 M_{\odot}$
Radius	$0.93 \pm 0.12 R_{\odot}$
Sp. Type	G5
Distance	$300 \pm 45 \text{ pc}$

**Notes:** Brightness magnitudes from Zacharias et al. [2013]. Mass and Radius estimate using the Torres et al. [2010] calibration. Spectral Type estimated from  $T_{\text{eff}}$  using the table in Gray [2008]. Abundances are relative to the solar values obtained by Asplund et al. [2009].

### 3.4.1 Stellar Age Estimates

Lithium is detected in the spectra of WASP-135, with an equivalent width of  $39 \text{ m\AA}$ , corresponding to an abundance of  $\log A(\text{Li}) = 2.01 \pm 0.06$ . This implies a stellar age of  $0.60_{-0.35}^{+1.40} \text{ Gyr}$  [Sestito and Randich, 2005].

The stellar rotation rate ( $P = 10.08 \pm 2.32 \text{ d}$ ) implied by the  $v \sin i$  from the spectral analysis gives a gyrochronological age of  $0.82_{-0.23}^{+0.41} \text{ Gyr}$  using the Barnes [2010] relation. This is an upper age limit as the  $v \sin i$  gives a minimum rotation rate.

Age estimates were also computed using several different stellar models for isochrone fitting using  $T_{\text{eff}}$  and the stellar density ( $\rho_*$ ) from the spectral analysis and the MCMC fit respectively. The method is described in Brown [2014]. The stellar data were fit to

isochrones at the central metallicity of  $[\text{Fe}/\text{H}]=0.02$ , and at the upper and lower limits. These results were combined to get the final estimates of the stellar age and mass. Three sets of stellar models were used: Padova isochrones as described in Marigo et al. [2008] and Girardi et al. [2010]; Yonsei-Yale isochrones as described in Demarque et al. [2004]; and Dartmouth (DSEP) isochrones as described in Dotter et al. [2008]. The ages calculated from these models ranged between about 3-6 Gyr, and can be found in Table 3.3 along with the associated stellar masses found with the models. The weighted mean and standard error of the three isochronal ages was found to be  $4.4 \pm 2.5$  Gyr. There is a discrepancy between the two young, fairly consistent ages from gyrochronology and Lithium abundances, and the older age estimates from isochrone fitting.

**Table 3.3:** Stellar age estimates for WASP-135.

Method	Age (Gyr)	Stellar Mass
Padova isochrones	$4.21^{+6.08}_{-6.70}$	$0.99^{+0.12}_{-0.09}$
Yonsei-Yale isochrones	$3.10^{+4.72}_{-2.56}$	$1.01^{+0.08}_{-0.08}$
DSEP isochrones	$5.96^{+3.91}_{-4.01}$	$0.95^{+0.08}_{-0.07}$
Average isochronal age	$4.4 \pm 2.5$	
Li abundance	$0.60^{+1.40}_{-0.35}$	
Gyrochronology (upper limit)	$0.82^{+0.41}_{-0.23}$	

**Note:** Padova isochrones described in Marigo et al. [2008] and Girardi et al. [2010]; Yonsei-Yale isochrones described in Demarque et al. [2004]; Dartmouth (DSEP) isochrones described in Dotter et al. [2008]; Gyrochronological age from Barnes [2010] relation; Li abundance age estimated from Sestito and Randich [2005].

### 3.5 MCMC System Parameters

All photometry data from WASP, along with the 3 nights of NITES data and 19 radial velocity measurements from SOPHIE were used in a Markov chain Monte Carlo (MCMC) fit. However, because the photometry from WASP was diluted by other stars inside and on the edge of the aperture, the transit depth in this data set was smaller than that found with NITES by a factor of 2.7. The in-transit WASP data was therefore corrected by this factor before the MCMC fitting, as has been done for other WASP planets, for example in Anderson et al. [2012]. This allowed the WASP data to constrain the ephemeris timing without affecting the transit depth.

The MCMC simultaneously fits a Keplerian orbital solution to the radial velocity data, and the Mandel and Agol [2002] model to the photometric transits. Limb-darkening was accounted for using a non-linear model with four coefficients, which were found

by interpolating from the R-band table of Claret [2000] and Claret [2004], which is appropriate for the NITES photometry.

We used an updated version of the code described in detail in Collier Cameron et al. [2007], Pollacco et al. [2008] and Brown et al. [2012], to fit for the following parameters: the epoch of mid-transit,  $T_0$ ; the orbital period,  $P$ ; the total transit duration,  $T_{14}$ ; the ingress/egress duration,  $T_{12}=T_{34}$ ; the planet to star area ratio,  $R_p^2/R_*^2$ ; the impact parameter for a circular orbit,  $b$ ;  $T_{\text{eff}}$ ;  $[\text{Fe}/\text{H}]$ , and the RV semi-amplitude,  $K$ . We applied priors on  $v \sin i$ ,  $T_{\text{eff}}$  and  $[\text{Fe}/\text{H}]$  using the values listed in Table 3.2, and a  $0.025 \text{ km s}^{-1}$  stellar jitter term was included in the fit. The output of the MCMC chains can be seen in Figure 3.4. The Lucy and Sweeney [1971] F-test was used to test for eccentricity in the Keplerian orbit. When the orbit was not forced to be circular in the MCMC fit, an eccentricity of  $0.038 \pm 0.011$  was found. According to the F-test the probability that this eccentricity could be found by chance is 0.059, therefore a circular model is adopted in the final MCMC analysis, as recommended in Anderson et al. [2012]. The resulting system parameters from this analysis are presented in Table 3.4.

**Table 3.4:** MCMC system parameters for WASP-135

Parameter	Value
$P$ (d)	$1.4013794 \pm 0.0000008$
$T_c$ BJD <sub>TDB</sub>	$2455230.9902 \pm 0.0009$
$T_{14}$ (d)	$0.069 \pm 0.001$
$T_{12} = T_{34}$ (d)	$0.018 \pm 0.002$
$\Delta F = R_p^2/R_*^2$	$0.0194 \pm 0.0008$
$b$	$0.80 \pm 0.03$
$i(^{\circ})$	$82.0 \pm 0.6$
$K_1(\text{km s}^{-1})$	$0.346 \pm 0.003$
$\gamma(\text{km s}^{-1})$	$-32.334 \pm 0.002$
$e$	0 (adopted)
$M_*(M_{\odot})$	$0.98 \pm 0.06$
$R_*(R_{\odot})$	$0.96 \pm 0.05$
$\log g_*$ (cgs)	$4.47 \pm 0.03$
$\rho_*(\rho_{\odot})$	$1.12 \pm 0.15$
$T_{\text{eff}}(\text{K})$	$5675 \pm 60$
$M_P(M_{\text{Jup}})$	$1.90 \pm 0.08$
$R_P(R_{\text{Jup}})$	$1.30 \pm 0.09$
$\log g_P$ (cgs)	$3.41 \pm 0.05$
$\rho_P(\rho_J)$	$0.87 \pm 0.17$
$a$ (AU)	$0.0243 \pm 0.0005$

Note: Errors are  $1\sigma$ ; Limb-darkening coefficients are:  $a_1 = 0.664$ ,  $a_2 = -0.378$ ,  
 $a_3 = 0.945$ ,  $a_4 = -0.470$

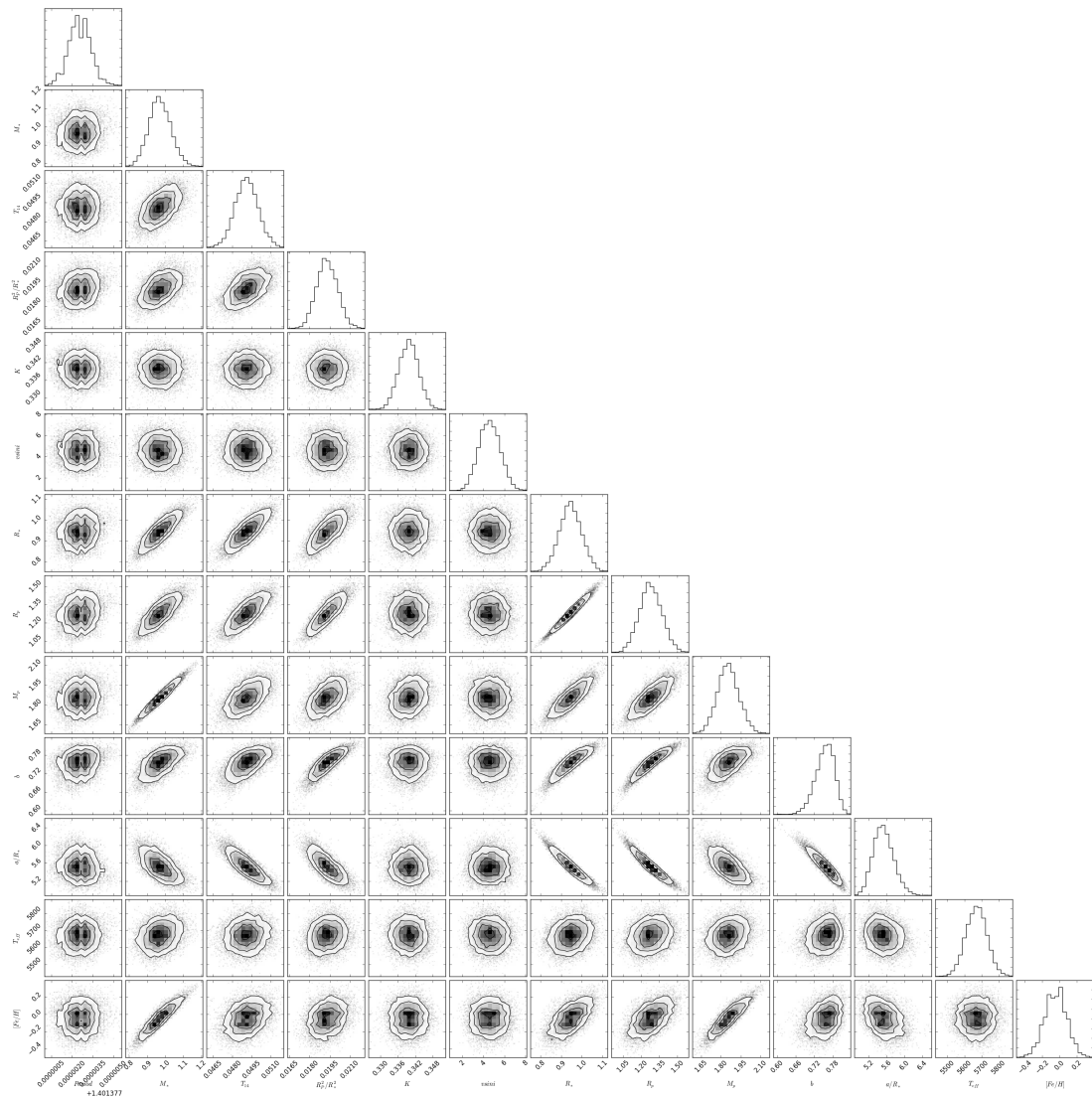


**Figure 3.4:** Output from MCMC chains, showing correlations between system parameters. Strong correlations can be seen between highly degenerate parameters in the transit and Keplerian models, such as  $M_*$  and  $M_p$ , or  $R_*$  and  $R_p$ .

## Chapter 4

# Conclusion

With a large radius of  $1.30 \pm 0.09 R_{\text{Jup}}$ , WASP-135b appears to be a bloated hot Jupiter. It is a highly irradiated exoplanet, receiving an insolation of  $1.98 \pm 0.24 \times 10^9 \text{ erg s}^{-1} \text{ cm}^{-2}$ , which is an order of magnitude greater than the cut off point found by Demory and Seager [2011] of  $\sim 2 \times 10^8 \text{ erg s}^{-1} \text{ cm}^{-2}$  (this can be seen in Figure 4.1). They find that giant planets receiving more insolation than this limit have inflated radii. Additionally, Weiss et al. [2013] find strong evidence for the dependence of giant planet radius on incident flux. Their empirical relation for planet radius, mass, and incident flux predicts a radius of  $1.30 \pm 0.07 R_{\text{Jup}}$  for WASP-135b, which fully agrees with the value measured in this work.

The weighted mean and standard error of the three isochronal ages for WASP-135 presented here (see table 3.3) is  $4.4 \pm 2.5 \text{ Gyr}$ , whilst the gyrochronological age upper limit is  $0.82_{-0.23}^{+0.41} \text{ Gyr}$ . This age discrepancy could be evidence of tidal spin-up of the star, due to its massive, short period planet. On the other hand, lithium is detected in the stellar spectrum, and the age estimate of  $0.60_{-0.35}^{+1.40} \text{ Gyr}$  from its abundance measurement lies below the upper age limit from gyrochronological models. Since the errors on the isochronal ages are large, and the gyrochronological and lithium ages agree well, the evidence for stellar spin-up appears weak, suggesting that WASP-135 is likely a relatively young star. Of the 146 exoplanets with masses greater than  $0.1 M_{\text{Jup}}$ , orbital distances less than 0.1 AU, and published estimates for their stellar host age, only 7 orbit stars younger than 0.8 Gyr<sup>1</sup>.

---

<sup>1</sup>exoplanetarchive.ipac.caltech.edu

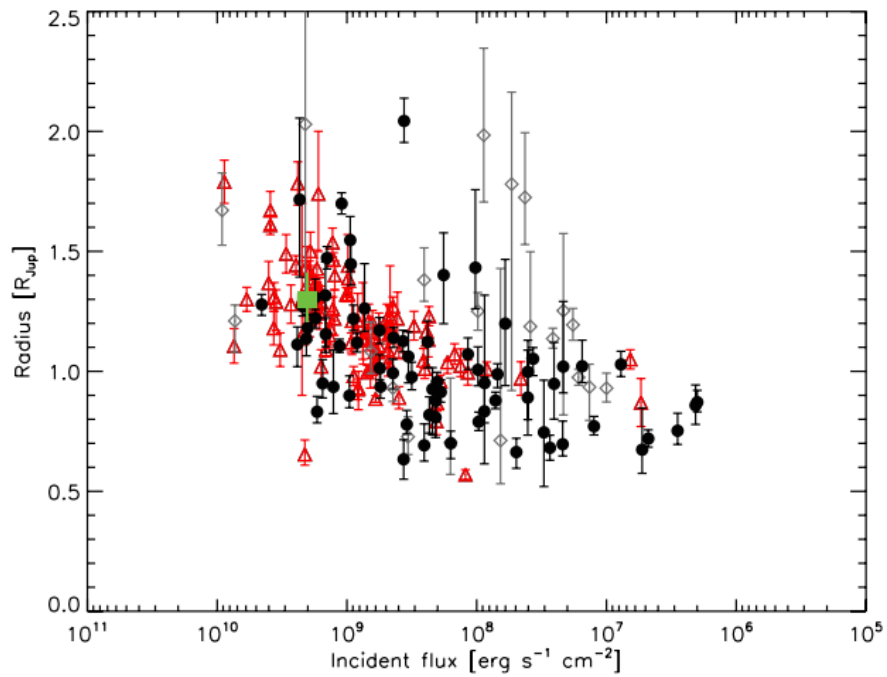


**Figure 4.1:** Planetary radii as a function of incident flux, from Demory and Seager [2011]. Same as Figure 1.2, with the inflated planet WASP-135b added as a green square. Before the cut-off point of  $\sim 2 \times 10^8 \text{ erg s}^{-1} \text{cm}^{-2}$  there is a correlation between planet radius and incident stellar flux.

# Bibliography

- H. S. Zepolsky and E. E. Salpeter. The Mass-Radius Relation for Cold Spheres of Low Mass. *ApJ*, 158:809, November 1969. doi: 10.1086/150240.
- B.-O. Demory and S. Seager. Lack of Inflated Radii for Kepler Giant Planet Candidates Receiving Modest Stellar Irradiation. *ApJS*, 197:12, November 2011. doi: 10.1088/0067-0049/197/1/12.
- M. Mayor and D. Queloz. A Jupiter-mass companion to a solar-type star. *Nature*, 378:355–359, November 1995. doi: 10.1038/378355a0.
- A. F. Martínez Fiorenzano, R. G. Gratton, S. Desidera, R. Cosentino, and M. Endl. Line bisectors and radial velocity jitter from SARG spectra. *A&A*, 442:775–784, November 2005. doi: 10.1051/0004-6361:20052888.
- K. Mandel and E. Agol. Analytic Light Curves for Planetary Transit Searches. *ApJ*, 580:L171–L175, December 2002. doi: 10.1086/345520.
- Giordano Bruno. *De l'infinito universo et mundi (On the infinite universe and worlds)*. 1584.
- E. A. Petigura, A. W. Howard, and G. W. Marcy. Prevalence of Earth-size planets orbiting Sun-like stars. *Proceedings of the National Academy of Science*, 110:19273–19278, November 2013.
- C. D. Dressing and D. Charbonneau. The Occurrence of Potentially Habitable Planets Orbiting M Dwarfs Estimated from the Full Kepler Dataset and an Empirical Measurement of the Detection Sensitivity. *ApJ*, 807:45, July 2015. doi: 10.1088/0004-637X/807/1/45.
- D. Charbonneau, T. M. Brown, R. W. Noyes, and R. L. Gilliland. Detection of an Extrasolar Planet Atmosphere. *ApJ*, 568:377–384, March 2002. doi: 10.1086/338770.
- D. K. Sing, H. R. Wakeford, A. P. Showman, N. Nikolov, J. J. Fortney, A. S. Burrows, G. E. Ballester, D. Deming, S. Aigrain, J.-M. Désert, N. P. Gibson, G. W. Henry, H. Knutson, A. Lecavelier des Etangs, F. Pont, A. Vidal-Madjar, M. W. Williamson,

- and P. A. Wilson. HST hot-Jupiter transmission spectral survey: detection of potassium in WASP-31b along with a cloud deck and Rayleigh scattering. *MNRAS*, 446: 2428–2443, January 2015. doi: 10.1093/mnras/stu2279.
- T. Louden and P. J. Wheatley. Spatially resolved eastward winds and rotation of HD 189733b. *ArXiv e-prints*, November 2015.
- J. J. Spake, D. J. A. Brown, A. P. Doyle, G. Hébrard, J. McCormac, D. J. Armstrong, D. Pollacco, Y. Gómez Maqueo Chew, D. R. Anderson, S. C. C. Barros, F. Bouchy, P. Boumis, G. Bruno, A. Collier Cameron, B. Courcol, G. R. Davies, F. Faedi, C. Hellier, J. Kirk, K. W. F. Lam, A. Liakos, T. Louden, P. F. L. Maxted, H. P. Osborn, E. Palle, J. Prieto Arranz, S. Udry, S. R. Walker, R. G. West, and P. J. Wheatley. WASP-135b: a highly irradiated, inflated hot Jupiter orbiting a G5V star. *ArXiv e-prints*, November 2015.
- L. Hebb, A. Collier-Cameron, A. H. M. J. Triaud, T. A. Lister, B. Smalley, P. F. L. Maxted, C. Hellier, D. R. Anderson, D. Pollacco, M. Gillon, D. Queloz, R. G. West, S. Bentley, B. Enoch, C. A. Haswell, K. Horne, M. Mayor, F. Pepe, D. Segransan, I. Skillen, S. Udry, and P. J. Wheatley. WASP-19b: The Shortest Period Transiting Exoplanet Yet Discovered. *ApJ*, 708:224–231, January 2010. doi: 10.1088/0004-637X/708/1/224.
- J. B. Pollack, O. Hubickyj, P. Bodenheimer, J. J. Lissauer, M. Podolak, and Y. Greenzweig. Formation of the Giant Planets by Concurrent Accretion of Solids and Gas. *Icarus*, 124:62–85, November 1996. doi: 10.1006/icar.1996.0190.
- J. J. Fortney and N. Nettelmann. The Interior Structure, Composition, and Evolution of Giant Planets. *Space Sci. Rev.*, 152:423–447, May 2010. doi: 10.1007/s11214-009-9582-x.
- I. Baraffe, G. Chabrier, and T. Barman. The physical properties of extra-solar planets. *Reports on Progress in Physics*, 73(1):016901, January 2010. doi: 10.1088/0034-4885/73/1/016901.
- B. Enoch, A. C. Cameron, D. R. Anderson, T. A. Lister, C. Hellier, P. F. L. Maxted, D. Queloz, B. Smalley, A. H. M. J. Triaud, R. G. West, D. J. A. Brown, M. Gillon, L. Hebb, M. Lendl, N. Parley, F. Pepe, D. Pollacco, D. Segransan, E. Simpson, R. A. Street, and S. Udry. WASP-25b: a 0.6  $M_J$  planet in the Southern hemisphere. *MNRAS*, 410:1631–1636, January 2011. doi: 10.1111/j.1365-2966.2010.17550.x.
- L. M. Weiss, G. W. Marcy, J. F. Rowe, A. W. Howard, H. Isaacson, J. J. Fortney, N. Miller, B.-O. Demory, D. A. Fischer, E. R. Adams, A. K. Dupree, S. B. Howell, R. Kolbl, J. A. Johnson, E. P. Horch, M. E. Everett, D. C. Fabrycky, and S. Seager.

- The Mass of KOI-94d and a Relation for Planet Radius, Mass, and Incident Flux. *ApJ*, 768:14, May 2013. doi: 10.1088/0004-637X/768/1/14.
- K. Batygin and D. J. Stevenson. Inflating Hot Jupiters with Ohmic Dissipation. *ApJ*, 714:L238–L243, May 2010. doi: 10.1088/2041-8205/714/2/L238.
- T. Guillot and A. P. Showman. Evolution of “51 Pegasus b-like” planets. *A&A*, 385: 156–165, April 2002. doi: 10.1051/0004-6361:20011624.
- A. F. Lanza. Hot Jupiters and the evolution of stellar angular momentum. *A&A*, 512: A77, March 2010. doi: 10.1051/0004-6361/200912789.
- F. Pont. Empirical evidence for tidal evolution in transiting planetary systems. *MNRAS*, 396:1789–1796, July 2009. doi: 10.1111/j.1365-2966.2009.14868.x.
- D. J. A. Brown. Discrepancies between isochrone fitting and gyrochronology for exoplanet host stars? *MNRAS*, 442:1844–1862, August 2014. doi: 10.1093/mnras/stu950.
- P. F. L. Maxted, A. M. Serenelli, and J. Southworth. A comparison of gyrochronological and isochronal age estimates for transiting exoplanet host stars. *ArXiv e-prints*, March 2015.
- G. Chauvin, A.-M. Lagrange, C. Dumas, B. Zuckerman, D. Mouillet, I. Song, J.-L. Beuzit, and P. Lowrance. A giant planet candidate near a young brown dwarf. Direct VLT/NACO observations using IR wavefront sensing. *A&A*, 425:L29–L32, October 2004. doi: 10.1051/0004-6361:200400056.
- C. Marois, B. Macintosh, T. Barman, B. Zuckerman, I. Song, J. Patience, D. Lafrenière, and R. Doyon. Direct Imaging of Multiple Planets Orbiting the Star HR 8799. *Science*, 322:1348, November 2008. doi: 10.1126/science.1166585.
- L. Lindgren and M. A. C. Perryman. GAIA: Global astrometric interferometer for astrophysics. *A&AS*, 116:579–595, May 1996.
- M. Perryman, J. Hartman, G. Á. Bakos, and L. Lindgren. Astrometric Exoplanet Detection with Gaia. *ApJ*, 797:14, December 2014. doi: 10.1088/0004-637X/797/1/14.
- D. L. Pollacco, I. Skillen, A. Collier Cameron, D. J. Christian, C. Hellier, J. Irwin, T. A. Lister, R. A. Street, R. G. West, D. R. Anderson, W. I. Clarkson, H. Deeg, B. Enoch, A. Evans, A. Fitzsimmons, C. A. Haswell, S. Hodgkin, K. Horne, S. R. Kane, F. P. Keenan, P. F. L. Maxted, A. J. Norton, J. Osborne, N. R. Parley, R. S. I. Ryans, B. Smalley, P. J. Wheatley, and D. M. Wilson. The WASP Project and the SuperWASP Cameras. *PASP*, 118:1407–1418, October 2006. doi: 10.1086/508556.

- G. Bakos, R. W. Noyes, G. Kovács, K. Z. Stanek, D. D. Sasselov, and I. Domsa. Wide-Field Millimagnitude Photometry with the HAT: A Tool for Extrasolar Planet Detection. *PASP*, 116:266–277, March 2004. doi: 10.1086/382735.
- W. J. Borucki, D. Koch, G. Basri, N. Batalha, T. Brown, D. Caldwell, J. Caldwell, J. Christensen-Dalsgaard, W. D. Cochran, E. DeVore, E. W. Dunham, A. K. Dupree, T. N. Gautier, J. C. Geary, R. Gilliland, A. Gould, S. B. Howell, J. M. Jenkins, Y. Kondo, D. W. Latham, G. W. Marcy, S. Meibom, H. Kjeldsen, J. J. Lissauer, D. G. Monet, D. Morrison, D. Sasselov, J. Tarter, A. Boss, D. Brownlee, T. Owen, D. Buzasi, D. Charbonneau, L. Doyle, J. Fortney, E. B. Ford, M. J. Holman, S. Seager, J. H. Steffen, W. F. Welsh, J. Rowe, H. Anderson, L. Buchhave, D. Ciardi, L. Walkowicz, W. Sherry, E. Horch, H. Isaacson, M. E. Everett, D. Fischer, G. Torres, J. A. Johnson, M. Endl, P. MacQueen, S. T. Bryson, J. Dotson, M. Haas, J. Kolodziejczak, J. Van Cleve, H. Chandrasekaran, J. D. Twicken, E. V. Quintana, B. D. Clarke, C. Allen, J. Li, H. Wu, P. Tenenbaum, E. Verner, F. Bruhweiler, J. Barnes, and A. Prsa. Kepler Planet-Detection Mission: Introduction and First Results. *Science*, 327:977, February 2010. doi: 10.1126/science.1185402.
- S. B. Howell, C. Sobeck, M. Haas, M. Still, T. Barclay, F. Mullally, J. Troeltzsch, S. Aigrain, S. T. Bryson, D. Caldwell, W. J. Chaplin, W. D. Cochran, D. Huber, G. W. Marcy, A. Miglio, J. R. Najita, M. Smith, J. D. Twicken, and J. J. Fortney. The K2 Mission: Characterization and Early Results. *PASP*, 126:398–408, April 2014. doi: 10.1086/676406.
- G. Kovács, S. Zucker, and T. Mazeh. A box-fitting algorithm in the search for periodic transits. *A&A*, 391:369–377, August 2002. doi: 10.1051/0004-6361:20020802.
- D. Foreman-Mackey, B. T. Montet, D. W. Hogg, T. D. Morton, D. Wang, and B. Schölkopf. A Systematic Search for Transiting Planets in the K2 Data. *ApJ*, 806:215, June 2015. doi: 10.1088/0004-637X/806/2/215.
- D. Bayliss, S. Hojjatpanah, A. Santerne, D. Dragomir, G. Zhou, A. Shporer, K. D. Colón, J. Almenara, D. J. Armstrong, D. Barrado, S. C. C. Barros, J. Bento, I. Boisse, F. Bouchy, D. J. A. Brown, T. Brown, A. Cameron, W. D. Cochran, O. Demangeon, M. Deleuil, R. F. Díaz, B. Fulton, K. Horne, G. Hébrard, J. Lillo-Box, C. Lovis, D. Mawet, H. Ngo, H. Osborn, E. Palte, E. Petigura, D. Pollacco, N. Santos, R. Sefako, R. Siverd, S. G. Sousa, and M. Tsantaki. EPIC201702477b: A Long Period Transiting Brown Dwarf from K2. *ArXiv e-prints*, June 2016.
- D. R. Anderson, A. Collier Cameron, C. Hellier, M. Lendl, P. F. L. Maxted, D. Pollacco, D. Queloz, B. Smalley, A. M. S. Smith, I. Todd, A. H. M. J. Triaud, R. G. West, S. C. C. Barros, B. Enoch, M. Gillon, T. A. Lister, F. Pepe, D. Ségransan, R. A.

- Street, and S. Udry. WASP-30b: A 61 M  $J_{up}$  Brown Dwarf Transiting a  $V = 12$ , F8 Star. *ApJ*, 726:L19, January 2011. doi: 10.1088/2041-8205/726/2/L19.
- R. J. Siverd, T. G. Beatty, J. Pepper, J. D. Eastman, K. Collins, A. Bieryla, D. W. Latham, L. A. Buchhave, E. L. N. Jensen, J. R. Crepp, R. Street, K. G. Stassun, B. S. Gaudi, P. Berlind, M. L. Calkins, D. L. DePoy, G. A. Esquerdo, B. J. Fulton, G. Fűrész, J. C. Geary, A. Gould, L. Hebb, J. F. Kielkopf, J. L. Marshall, R. Pogge, K. Z. Stanek, R. P. Stefanik, A. H. Szentgyorgyi, M. Trueblood, P. Trueblood, A. M. Stutz, and J. L. van Saders. KELT-1b: A Strongly Irradiated, Highly Inflated, Short Period, 27 Jupiter-mass Companion Transiting a Mid-F Star. *ApJ*, 761:123, December 2012. doi: 10.1088/0004-637X/761/2/123.
- E. Kruse and E. Agol. KOI-3278: A Self-Lensing Binary Star System. *Science*, 344: 275–277, April 2014. doi: 10.1126/science.1251999.
- C. G. Toner and D. F. Gray. The starpatch on the G8 dwarf XI Bootis A. *ApJ*, 334: 1008–1020, November 1988. doi: 10.1086/166893.
- S. Seager and G. Mallén-Ornelas. A Unique Solution of Planet and Star Parameters from an Extrasolar Planet Transit Light Curve. *ApJ*, 585:1038–1055, March 2003. doi: 10.1086/346105.
- E. B. Ford. Quantifying the Uncertainty in the Orbits of Extrasolar Planets. *AJ*, 129: 1706–1717, March 2005. doi: 10.1086/427962.
- N. Zacharias, C. T. Finch, T. M. Girard, A. Henden, J. L. Bartlett, D. G. Monet, and M. I. Zacharias. The Fourth US Naval Observatory CCD Astrograph Catalog (UCAC4). *AJ*, 145:44, February 2013. doi: 10.1088/0004-6256/145/2/44.
- A. Collier Cameron, D. Pollacco, R. A. Street, T. A. Lister, R. G. West, D. M. Wilson, F. Pont, D. J. Christian, W. I. Clarkson, B. Enoch, A. Evans, A. Fitzsimmons, C. A. Haswell, C. Hellier, S. T. Hodgkin, K. Horne, J. Irwin, S. R. Kane, F. P. Keenan, A. J. Norton, N. R. Parley, J. Osborne, R. Ryans, I. Skillen, and P. J. Wheatley. A fast hybrid algorithm for exoplanetary transit searches. *MNRAS*, 373:799–810, December 2006. doi: 10.1111/j.1365-2966.2006.11074.x.
- D. Pollacco, I. Skillen, A. Collier Cameron, B. Loeillet, H. C. Stempels, F. Bouchy, N. P. Gibson, L. Hebb, G. Hébrard, Y. C. Joshi, I. McDonald, B. Smalley, A. M. S. Smith, R. A. Street, S. Udry, R. G. West, D. M. Wilson, P. J. Wheatley, S. Aigrain, K. Alsubai, C. R. Benn, V. A. Bruce, D. J. Christian, W. I. Clarkson, B. Enoch, A. Evans, A. Fitzsimmons, C. A. Haswell, C. Hellier, S. Hickey, S. T. Hodgkin, K. Horne, M. Hrudková, J. Irwin, S. R. Kane, F. P. Keenan, T. A. Lister, P. Maxted, M. Mayor, C. Moutou, A. J. Norton, J. P. Osborne, N. Parley, F. Pont, D. Queloz, R. Ryans, and

- E. Simpson. WASP-3b: a strongly irradiated transiting gas-giant planet. *MNRAS*, 385:1576–1584, April 2008. doi: 10.1111/j.1365-2966.2008.12939.x.
- A. M. S. Smith, L. Hebb, A. Collier Cameron, D. R. Anderson, T. A. Lister, C. Hellier, D. Pollacco, D. Queloz, I. Skillen, and R. G. West. A SuperWASP search for additional transiting planets in 24 known systems. *MNRAS*, 398:1827–1834, October 2009. doi: 10.1111/j.1365-2966.2009.15262.x.
- P. F. L. Maxted, D. R. Anderson, A. Collier Cameron, C. Hellier, D. Queloz, B. Smalley, R. A. Street, A. H. M. J. Triaud, R. G. West, M. Gillon, T. A. Lister, F. Pepe, D. Pollacco, D. Ségransan, A. M. S. Smith, and S. Udry. WASP-41b: A Transiting Hot Jupiter Planet Orbiting a Magnetically Active G8V Star. *PASP*, 123:547–554, May 2011. doi: 10.1086/660007.
- J. Eastman, R. Siverd, and B. S. Gaudi. Achieving Better Than 1 Minute Accuracy in the Heliocentric and Barycentric Julian Dates. *PASP*, 122:935–946, August 2010. doi: 10.1086/655938.
- F. Bouchy, G. Hébrard, S. Udry, X. Delfosse, I. Boisse, M. Desort, X. Bonfils, A. Eggenberger, D. Ehrenreich, T. Forveille, A. M. Lagrange, H. Le Coroller, C. Lovis, C. Moutou, F. Pepe, C. Perrier, F. Pont, D. Queloz, N. C. Santos, D. Ségransan, and A. Vidal-Madjar. The SOPHIE search for northern extrasolar planets . I. A companion around HD 16760 with mass close to the planet/brown-dwarf transition. *A&A*, 505:853–858, October 2009. doi: 10.1051/0004-6361/200912427.
- A. Baranne, D. Queloz, M. Mayor, G. Adrianzyk, G. Knispel, D. Kohler, D. Lacroix, J.-P. Meunier, G. Rimbaud, and A. Vin. ELODIE: A spectrograph for accurate radial velocity measurements. *A&AS*, 119:373–390, October 1996.
- F. Pepe, M. Mayor, F. Galland, D. Naef, D. Queloz, N. C. Santos, S. Udry, and M. Burnet. The CORALIE survey for southern extra-solar planets VII. Two short-period Saturnian companions to  $\mu$ ASTROBJ HD 108147/ASTROBJ and  $\mu$ ASTROBJ HD 168746/ASTROBJ. *A&A*, 388:632–638, June 2002. doi: 10.1051/0004-6361:20020433.
- I. Boisse, A. Eggenberger, N. C. Santos, C. Lovis, F. Bouchy, G. Hébrard, L. Arnold, X. Bonfils, X. Delfosse, M. Desort, R. F. Díaz, D. Ehrenreich, T. Forveille, A. Gallenne, A. M. Lagrange, C. Moutou, S. Udry, F. Pepe, C. Perrier, S. Perruchot, F. Pont, D. Queloz, A. Santerne, D. Ségransan, and A. Vidal-Madjar. The SOPHIE search for northern extrasolar planets. III. A Jupiter-mass companion around HD 109246. *A&A*, 523:A88, November 2010. doi: 10.1051/0004-6361/201014909.

- D. Queloz, G. W. Henry, J. P. Sivan, S. L. Baliunas, J. L. Beuzit, R. A. Donahue, M. Mayor, D. Naef, C. Perrier, and S. Udry. No planet for HD 166435. *A&A*, 379:279–287, November 2001. doi: 10.1051/0004-6361:20011308.
- J. McCormac, D. Pollacco, I. Skillen, F. Faedi, I. Todd, and C. A. Watson. DONUTS: A Science Frame Autoguiding Algorithm with Sub-Pixel Precision, Capable of Guiding on Defocused Stars. *PASP*, 125:548–556, May 2013.
- J. McCormac, I. Skillen, D. Pollacco, F. Faedi, G. Ramsay, V. S. Dhillon, I. Todd, and A. Gonzalez. A search for photometric variability towards M71 with the Near-Infrared Transiting ExoplanetS Telescope. *MNRAS*, 438:3383–3398, March 2014. doi: 10.1093/mnras/stt2449.
- P. B. Stetson. DAOPHOT - A computer program for crowded-field stellar photometry. *PASP*, 99:191–222, March 1987. doi: 10.1086/131977.
- A. P. Doyle, B. Smalley, P. F. L. Maxted, D. R. Anderson, A. C. Cameron, M. Gillon, C. Hellier, D. Pollacco, D. Queloz, A. H. M. J. Triaud, and R. G. West. Accurate spectroscopic parameters of WASP planet host stars. *MNRAS*, 428:3164–3172, February 2013. doi: 10.1093/mnras/sts267.
- P. Magain. A comment on systematic errors in determinations of microturbulent velocities. *A&A*, 134:189–192, May 1984.
- U. Munari and T. Zwitter. Equivalent width of NA I and K I lines and reddening. *A&A*, 318:269–274, February 1997.
- A. P. Doyle, G. R. Davies, B. Smalley, W. J. Chaplin, and Y. Elsworth. Determining stellar macroturbulence using asteroseismic rotational velocities from Kepler. *MNRAS*, 444:3592–3602, November 2014. doi: 10.1093/mnras/stu1692.
- G. Torres, J. Andersen, and A. Giménez. Accurate masses and radii of normal stars: modern results and applications. *A&A Rev.*, 18:67–126, February 2010. doi: 10.1007/s00159-009-0025-1.
- D. F. Gray. *The observation and analysis of stellar photospheres*. Cambridge University Press, 3rd edition, 2008.
- M. Asplund, N. Grevesse, A. J. Sauval, and P. Scott. The Chemical Composition of the Sun. *ARA&A*, 47:481–522, September 2009. doi: 10.1146/annurev.astro.46.060407.145222.
- P. Sestito and S. Randich. Time scales of Li evolution: a homogeneous analysis of open clusters from ZAMS to late-MS. *A&A*, 442:615–627, November 2005. doi: 10.1051/0004-6361:20053482.

- S. A. Barnes. A Simple Nonlinear Model for the Rotation of Main-sequence Cool Stars. I. Introduction, Implications for Gyrochronology, and Color-Period Diagrams. *ApJ*, 722:222–234, October 2010. doi: 10.1088/0004-637X/722/1/222.
- P. Marigo, L. Girardi, A. Bressan, M. A. T. Groenewegen, L. Silva, and G. L. Granato. Evolution of asymptotic giant branch stars. II. Optical to far-infrared isochrones with improved TP-AGB models. *A&A*, 482:883–905, May 2008. doi: 10.1051/0004-6361:20078467.
- L. Girardi, B. F. Williams, K. M. Gilbert, P. Rosenfield, J. J. Dalcanton, P. Marigo, M. L. Boyer, A. Dolphin, D. R. Weisz, J. Melbourne, K. A. G. Olsen, A. C. Seth, and E. Skillman. The ACS Nearby Galaxy Survey Treasury. IX. Constraining Asymptotic Giant Branch Evolution with Old Metal-poor Galaxies. *ApJ*, 724:1030–1043, December 2010. doi: 10.1088/0004-637X/724/2/1030.
- P. Demarque, J.-H. Woo, Y.-C. Kim, and S. K. Yi.  $Y^2$  Isochrones with an Improved Core Overshoot Treatment. *ApJS*, 155:667–674, December 2004. doi: 10.1086/424966.
- A. Dotter, B. Chaboyer, D. Jevremović, V. Kostov, E. Baron, and J. W. Ferguson. The Dartmouth Stellar Evolution Database. *ApJS*, 178:89–101, September 2008. doi: 10.1086/589654.
- D. R. Anderson, A. Collier Cameron, M. Gillon, C. Hellier, E. Jehin, M. Lendl, P. F. L. Maxted, D. Queloz, B. Smalley, A. M. S. Smith, A. H. M. J. Triaud, R. G. West, F. Pepe, D. Pollacco, D. Ségransan, I. Todd, and S. Udry. WASP-44b, WASP-45b and WASP-46b: three short-period, transiting extrasolar planets. *MNRAS*, 422:1988–1998, May 2012. doi: 10.1111/j.1365-2966.2012.20635.x.
- A. Claret. A new non-linear limb-darkening law for LTE stellar atmosphere models. Calculations for  $-5.0 = \log[M/H] = +1$ ,  $2000 \text{ K} = T_{eff} = 50000 \text{ K}$  at several surface gravities. *A&A*, 363:1081–1190, November 2000.
- A. Claret. A new non-linear limb-darkening law for LTE stellar atmosphere models III. *A&A*, 428:1001–1005, December 2004. doi: 10.1051/0004-6361:20041673.
- A. Collier Cameron, D. M. Wilson, R. G. West, L. Hebb, X.-B. Wang, S. Aigrain, F. Bouchy, D. J. Christian, W. I. Clarkson, B. Enoch, M. Esposito, E. Guenther, C. A. Haswell, G. Hébrard, C. Hellier, K. Horne, J. Irwin, S. R. Kane, B. Loeillet, T. A. Lister, P. Maxted, M. Mayor, C. Moutou, N. Parley, D. Pollacco, F. Pont, D. Queloz, R. Ryans, I. Skillen, R. A. Street, S. Udry, and P. J. Wheatley. Efficient identification of exoplanetary transit candidates from SuperWASP light curves. *MNRAS*, 380:1230–1244, September 2007. doi: 10.1111/j.1365-2966.2007.12195.x.

- 
- D. J. A. Brown, A. Collier Cameron, R. F. Díaz, A. P. Doyle, M. Gillon, M. Lendl, B. Smalley, A. H. M. J. Triaud, D. R. Anderson, B. Enoch, C. Hellier, P. F. L. Maxted, G. R. M. Miller, D. Pollacco, D. Queloz, I. Boisse, and G. Hébrard. Analysis of Spin-Orbit Alignment in the WASP-32, WASP-38, and HAT-P-27/WASP-40 Systems. *ApJ*, 760:139, December 2012. doi: 10.1088/0004-637X/760/2/139.
- L. B. Lucy and M. A. Sweeney. Spectroscopic binaries with circular orbits. *AJ*, 76: 544–556, August 1971. doi: 10.1086/111159.